Frontiers in Bioscience Landmark

Front. Biosci. (Landmark Ed) **2024**; 29(7): 274
https://doi.org/10.31083/j.fbl2907274

Original Research

LARP7 Contributes to Glucose-Induced Cardiac Dysfunction, Apoptosis and Fibrosis by Inhibiting the Degradation of STING

Jingjing Sun[1,†], Ziming Wang[1,†], Yixuan Duan[1], Chang Liu[1], Sihai Zhao[2], Jie Deng[1,*]

[1]Department of Cardiology, The Second Affiliated Hospital of Xi'an Jiaotong University, 710004 Xi'an, Shaanxi, China
[2]Laboratory Animal Center, Xi'an Jiaotong University School of Medicine, 710061 Xi'an, Shaanxi, China
*Correspondence: jie.deng@mail.xjtu.edu.cn (Jie Deng)
[†]These authors contributed equally.

Academic Editor: Natascia Tiso
Submitted: 14 April 2024 Revised: 5 June 2024 Accepted: 13 June 2024 Published: 26 July 2024

Abstract

Background: Diabetic cardiomyopathy (DCM) is an important cause of heart failure in diabetic patients. The aim of this study was to investigate the pathogenesis of DCM and to identify potential therapeutic targets. **Methods**: A mouse model of type 1 DCM was constructed by continuous intraperitoneal injection of streptozotocin (STZ). Systolic and diastolic functions were measured by ultrasound. The expression of La-related protein 7 (LARP7), the stimulator of interferon genes (STING) pathway and light chain 3 (LC3) in myocardial tissue was detected by Western blot and immunofluorescence analyses. Neonatal mouse ventricular cardiomyocytes (NMVCMs) were isolated and cultured. An *in vitro* type 1 diabetes mellitus (T1DM) model was established by treatment with high glucose. Knockdown/overexpression of LARP7 and STING was achieved by adenovirus transduction, C-176 (a potent covalent inhibitor of STING), and plasmid transfection. The expression, activation, and localization of STING and LARP7 in cardiomyocytes was evaluated, as well as the interaction between the two. The effect of this interaction on the STING-dependent autophagy–lysosomal pathway was also explored. In addition, the fibrosis and apoptosis of cardiomyocytes were evaluated. **Results**: High glucose was found to increase the expression and activation of STING and LARP7 in mouse myocardial tissue. This was accompanied by myocardial fibrosis, impaired autophagy degradation function and impaired cardiac function. These findings were further confirmed by *in vitro* experiments. High glucose caused LARP7 to translocate from the nucleus to the cytoplasm, where it interacted with accumulated STING to inhibit its degradation. Inhibition of STING or LARP7 expression significantly improved myocardial injury induced by high glucose. **Conclusions**: Targeted inhibition of LARP7 or STING expression may be a potential therapeutic strategy for the treatment of DCM.

Keywords: diabetic cardiomyopathy; LARP7; STING; autophagy; apoptosis; fibrosis

1. Introduction

Diabetes mellitus (DM) is a major chronic disease that endangers human health. The cardiovascular damage caused by DM has become the main cause of death in diabetic patients [1]. Diabetic cardiomyopathy (DCM) is one of the cardiac complications of DM and refers to impaired cardiac filling and decreased systolic function, which ultimately induces heart failure [2,3]. Current treatment methods for DCM focus on controlling blood sugar, delaying ventricular remodeling, and correcting heart failure. However, there is still a lack of effective treatments for DCM. Conventional treatments place a heavy financieal burden on patients and have limitations. Despite the standardized application of drugs such as sodium-dependent glucose transporters 2 (SGLT2) inhibitors, spironolactone, angiotensin-converting enzyme inhibitors (ACEIs) and angiotensin II receptor blockers (ARBs), many diabetic patients still suffer end-stage heart failure due to DCM [4–7].

Stimulator of interferon gene (STING) is a signal transduction molecule closely associated with the innate immune response. It is induced by virus invasion and cell damage and activates the inflammatory response through the induction of type I interferons (IFN-I) to resist exotic pathogens [8]. Of note, pathogenic microbial DNA can induce the expression and activation of STING. Moreover, endogenous DNA release caused by various intracellular toxic stresses can have the same effect [9]. Increasing evidence suggests that STING plays an important role in regulating insulin sensitivity and inducing ventricular remodeling in diabetic patients. On one hand, activation of the STING pathway can affect the homeostasis of glucose metabolism by mediating pancreatic β-cell senescence, glucose intolerance, and insulin resistance [10]. On the other hand, during the progression of DCM, myocardial hypertrophy can be promoted by inducing pyroptosis and proinflammatory responses [11]. Under physiological conditions, STING can be degraded through various pathways after exerting its signal transduction function, such as the K48 ubiquitin–proteasome pathway and autophagy–lysosome pathway, thus avoiding tissue damage caused by its overexpression and activation [12–14]. Previous studies established that during the course of cardiovascular diseases such as myocardial infarction and heart failure, various pathogenic

factors can inhibit STING degradation, result in intracellular accumulation as well as causing overactivation of downstream signaling pathways [15–18]. The aim of the present study was therefore to explore the relationship between obstruction of the STING degradation pathway and the progression of DCM.

LARP7 is a member of the La-related protein (LARP) family. It acts as an important negative transcriptional regulator of RNA polymerase II and is also involved in the induction of ventricular hypertrophy [18,19]. More than 50% of LARP7 in human cells forms part of the 7SK complex, which includes 7SK RNA, methyl phosphate capping enzyme (MePCE), hexamethylene bis-acetamide inducible (HEXIM1/2), and positive transcription elongation factor b (P-TEFb). LARP7 binds to the C-terminal UUU-3′OH of 7SK RNA to maintain the stability of 7SK ribonucleoprotein (RNP), together with MePCE [20,21]. In myocardial tissue, pathological stimuli cause LARP7 to dissociate, thereby reducing the stability of the complex. Free P-TEFb is then recruited to the RNA polymerase II promoter by transcription factors such as bromodomain protein 4 (BRD4), thereby stimulating transcription elongation and inducing ventricular hypertrophy [22]. However, the role of free LARP7 in the cytoplasm is still unclear.

In the present study, a high glucose-induced DCM cell model was used to investigate the role of free LARP7 in the process of glucose-induced cardiac dysfunction, apoptosis and fibrosis. The results indicate that high glucose inhibits the degradation of STING through the autophagy-lysosomal pathway. Additionally, LARP7 expression was upregulated and its intracellular localization was altered. Moreover, the degradation of STING was inhibited by its interaction with LARP7. The accumulation of STING *in vivo* not only caused inflammation and immune responses, but also induced myocardial remodeling and cardiac dysfunction by inducing cardiomyocyte fibrosis and apoptosis. Downregulation of STING or LARP7 expression significantly inhibited the occurrence of fibrosis and apoptosis. This study identified a regulatory effect of free LARP7 on the STING pathway, thus providing new insights into the pathogenesis of DCM. Furthermore, it suggested that targeting of STING or LARP7, either alone or in combination, could serve as a novel therapeutic strategy for the treatment of DCM.

2. Materials and Methods

2.1 DCM Mouse Model

Male C57BL/6J mice (6–8 weeks old) were purchased from the Experimental Animal Center, Fourth Military Medical University (Xi'an, Shaanxi, China). Mice were randomly assigned to a control group and to a Type 1 diabetes mellitus (T1DM) group. An Streptozotocin (STZ) solution (Sigma-Aldrich, St. Louis, MO, USA, 60 mg/kg) was injected intraperitoneally for 5 consecutive days to construct a type 1 DCM mouse model. The control group was injected with an equal volume of citrate buffer. Blood samples were collected via the tail vein on days 3, 5 and 7 after the last injection. Mice with a random blood glucose level $\geq$16.7 mmol/L were considered to have type 1 DCM and were then maintained for another 6 weeks to develop myocardial injury. All animal experiments were performed in accordance with the guidelines of the Animal Experimentation Committee of the Second Affiliated Hospital of Xi'an Jiaotong University (Shaanxi, approved number XJTUAE2022-374), and all methods were carried out in accordance with Animal Research: Reporting in Vivo Experiments (ARRIVE) guidelines. The above-mentioned experiments were conducted at least three times.

2.2 Echocardiography

Mice were anesthetized with 2% isoflurane. Echocardiography was used to calculate cardiac function with the UBM system (Vevo 770, Toronto, Canada). Left ventricular fractional shortening (FS) and the ejection fraction (EF) were assessed using Vevo Analysis software (version 3.0.0, VisualSonics, Toronto, Canada). To assess diastolic function, an apical four-chamber view of the left ventricle was obtained. Maximal early (E) and late (A) transmitral velocities in diastole were analyzed to measure the mitral inflow velocity spectrum. Echocardiography was conducted by investigators who were blinded to the study.

2.3 Immunohistochemistry and Immunofluorescence

After the T1DM model was successfully constructed, mice were sacrificed by cervical dislocation. Left ventricular specimens were obtained, fixed with 4% paraformaldehyde and embedded in paraffin. Tissue samples from the myocardium were then cut into serial sections (5 µm thickness) from the mid-transverse area. The sections were heated to retrieve antigen and then incubated with anti-LC3 antibody overnight at 4 °C. After incubating with a universal two-step kit (anti-rabbit/anti-mouse PV-9000 secondary antibodies) at room temperature for 1 h, diaminobenzidine was used for color rendering and hematoxylin to stain the nuclei. Sections were then cleared in xylene and sealed with neutral gum. An isotype control antibody was used as the negative control. A digital scanner (Pannoramic MIDI, 3DHISTECH, Budapest, Hungary) was used to analyze the immunohistochemistry results. The sections were stained with picrosirus red to display the collagen components. Statistical analysis was carried out using the grading system described in the immunohistochemical technique method of the Chinese Pathological Society.

CY3-labeled STING, FITC-labeled LARP7, and 4′,6-diamidino-2-phenylindole (DAPI) were used in the immunofluorescence analysis. An anti-fluorescence quencher was used for mounting, and a laser confocal workstation was used for immunofluorescence photography. Semi-quantitative analysis of fluorescence images was performed using ImageJ software (version 1.6.0, National Institutes of Health (NIH), Bethesda, MD, USA).

2.4 Culture and Processing of Neonatal Mouse Ventricular Cardiomyocytes (NMVCMs)

Cardiomyocytes were obtained from the ventricles of 1–3-day old neonatal C57BL/6 mice. The mice were sterilized with 75% ethanol and the hearts removed and rinsed in ice-cold phosphate-buffered saline (PBS, Servicebio, Wuhan, China). The myocardial samples were then cut into small pieces and digested with collagenase type 2 (Sigma–Aldrich, Saint Louis, MO, USA) until the tissue pieces had dissolved. The suspension was then mixed with dulbecco's modified eagle medium (DMEM) (ScienCell, San Diego, CA, USA) to stop digestion. The mixture was centrifuged (800 $\times$g for 5 min) and the supernatant retained. The cardiomyocyte-enriched fraction was further resuspended in DMEM. Differential adhesion was used to separate cardiomyocytes and fibroblasts. The isolated cells were placed in a culture flask at 37 °C for 1 h so that fibroblasts could accumulate at the bottom. The cardiomyocytes remained suspended in the medium and were then cultured at 37 °C in 5% CO_2 in DMEM supplemented with 10% fetal bovine serum (SV30087.02, Hyclone, Logan, UT, USA) and 1% penicillin/streptomycin. Cells were seeded in 6-well plates (for Western blot assay) or 20 mm confocal dishes (for immunofluorescence) prior to transfection.

For the knockdown or overexpression of *LARP7*, NMVCMs were infected with adenovirus carrying negative control (NC-small interfering RNA (siRNA)), knockdown of rat *LARP7* gene (LARP7-siRNA), or overexpression of the *LARP7* gene (m-LARP7) at an MOI of 100 from Hanbio Tech (Shanghai, China). STING was exogenously overexpressed in NMVCMs via plasmid transfection (m-3*Flag-STING). The corresponding sequences were: LARP7-siRNA (5′-3′): TGAGAGACCAAAGGACGAGGA, CTTCTTCTGGTGGGTTGTTCAG; m-LARP7 (5′-3′): CCCAAGGCCAAAAGCTAAGAA, CTCAATGGTATAACCTCCTCGC. Gene expression levels for *LARP7* and STING were evaluated by real-time quantitative PCR, and the protein level by Western blot. Stably overexpressing STING, *LARP7* and low expression *LARP7* cells were selected for futher intervention with high glucose. NMVCMs were cultured with 33 mM glucose for 48 h to simulate a type 1 DCM model *in vitro* [23]. NMVCMs were treated for 2 h with the autophagy inhibitor 3-methyladenine (3-MA, 10mM) (A8353, APExBIO, Houston, TX, USA) to determine the effect of autophagy on apoptosis and STING expression. NMVCMs were also treated with 1 mM of C-176 (HY-112906, MedChemExpress, Shanghai, China), a potent covalent inhibitor of STING, to evaluate the role of STING in cardiomyocyte fibrosis and apoptosis. Cardiomyocytes were randomly divided into the following groups: (i) control; (ii) high glucose (HG); (iii) 3-MA; (iv) HG+C-176; (v) HG+LARP7-siRNA; (vi) HG+LARP7-siRNA+C-176; (vii) LARP7-siRNA; (viii) m-3*Flag-STING; (ix) m-3*Flag-STING+LARP7-siRNA; (x) HG+m-3*Flag-STING; (xi) HG+m-3*Flag-STING+LARP7-siRNA; and (xii) m-LARP7.

2.5 Western Blot Analysis

The cell medium from NMVCMs was discarded and the cells washed with PBS. The samples were then homogenized in pre-cooled protein lysis buffer containing phenylmethylsulfonyl fluoride (PMSF) (1 mM, pH = 7.4) (HY-B0496, MedChemExpress, Shanghai, China), lysed by ultrasound, and centrifuged for 30 min to extract total protein. Protein quantification was performed using the bicinchoninic acid assay (BCA) method. Total protein (20 µg) was electrophoresed on a 10% denaturing polyacrylamide gel and the separated proteines then transferred onto a polyvinylidene fluoride (PVDF) membrane. After blocking with 5% non-fat milk, the membrane was incubated overnight at 4 °C with the following primary antibodies: cGAS, p-STING (Ser365), STING, LARP7, INF-β, α-SMA, Cl-Caspase3, LC3II/I, Beclin-1 and P62 (as shown in **Supplementary Tables 1,2**). The membrane was subsequently incubated with horseradish peroxidase (HRP)-labeled secondary antibody (1:5000, Cell Signaling, Danvers, MA, USA) at room temperature for 40 min. Glyceraldehyde-3-phosphate dehydrogenase (GAPDH) and β-actin were used as loading controls. Blots were visualized with a chemiluminescence system (Amersham Bioscience, Buchinghamshire, UK) and semi-quantitative densitometry results obtained for the developed bands. The ratio of the gray value of the target band to that of the GAPDH band was calculated to evaluate the protein level.

2.6 α-SMA and Phalloidin Staining of Cardiomyocytes

To evaluate the extent of cardiomyocyte remodeling, α-SMA and phalloidin staining were used to analyze the degree of myocardial fibrosis and the cytoskeletal morphology, respectively. Confocal dishes pre-seeded with NMVCMs were washed three times with precooled PBS, and the cardiomyocytes then fixed for 15–20 min with formaldehyde precooled to 4 °C. This was followed by 3 washes with precooled PBS, and incubation in permeabilization buffer (0.1% Triton X-100 in PBS) for 15 min to rupture the cell membranes. Cells were then incubated with a bovine serum albumin (BSA) solution for 90 min to block nonspecific binding. Next, primary antibody against α-SMA was added and the cells incubated overnight at 4 °C. Fluorescent (FITC) secondary antibody (rabbit anti-mouse, 1:200, Boster) was then added and the cells incubated for 60 min at room temperature. DAPI was subsequently used for nuclear staining, while the expression of α-SMA in each group of cells was estimated from the intensity of green fluorescence in the field of view. Phalloidin staining was used to visually assess the morphology of the myocardial cytoskeleton by laser confocal microscopy and use of the appropriate fluorescence channel.

2.7 Cardiomyocyte Apoptosis

Cardiomyocyte apoptosis was assessed using the DNA ladder assay, terminal deoxynucleotidyl transferase mediated nick end labeling (TUNEL) staining, and Western blot analysis of Cl-caspase3. TUNEL staining was used to stain myocardial tissue sections, as recommended by the instructions provided with the apoptosis detection kit (Roche, Basel, Switzerland). After mounting with an antifluorescence quenching agent, the sections were observed and photographed under a laser confocal microscope (Leica TCS SP8, Leica, Hessen, Germany), thus allowing the cell apoptosis rate to be determined [24].

In the DNA ladder assay, myocardial DNA was extracted using a nucleic acid extraction kit (IsoQuicks, Microprobe, Carlsbad, CA, USA). The extracted DNA (10 mg) was added to a 2% agarose gel containing ethidium bromide and electrophoresed in Tris-borate-EDTA (TBE) buffer at 100 V for 2 h. The DNA ladders were then photographed.

2.8 Immunofluorescence Staining

The colocalization in cardiomyocytes of STING and LC3, and of STING and LARP7, were evaluated separately by immunofluorescence. NMVCMs were seeded into confocal dishes and then treated. The culture medium was discarded and the cells washed three times with sterile PBS, incubated in permeabilization buffer (0.1% Triton X-100 in PBS) for 15 min to rupture cell membranes, and incubated in a BSA solution for 60 min to block nonspecific binding. The cells were then incubated overnight at 4 °C with rabbit-derived STING, LC3 and LARP7 antibodies. Subsequently, the cells were incubated with an appropriate secondary antibody for 90 min at room temperature. Different molecules are labeled with different fluorescence which was evaluated using a laser confocal microscope. The extent of merging of different groups of fluorescent particles was analyzed and calculated using Image-Pro PLUS software (Media Cybernetics, Silver Spring, MD, USA) to evaluate the colocalization of STING and LC3, as well as that of STING and LARP7.

2.9 Coimmunoprecipitation (COIP) and Mass Spectrometry (MS)

COIP was conducted using a Proteintech immunoprecipitation (IP) kit (KIP-2). NMVCMs were pre-processed and grouped. To fully lyse cardiomyocytes, a total of 100 µL of precooled IP lysis buffer (containing 1× protease inhibitor) was added to 106 cells for 30 min. The cells were disrupted by ultrasonication for 1 min to fully lyse and fragment the DNA. They were then centrifuged at 12,000 rpm for 10 min at 4 °C and the supernatant collected. Washed Protein A-Sepharose beads (30 µL) were then added to each lysate tube, and the samples incubated for 120 min with slow rotation at 4 °C. This was followed by centrifugation at 12,000 rpm for 1 min, after which the supernatant was collected and 4 µg of IP antibody and 300 µL of incubation buffer were added to the supernatant. As a negative control, equal amounts of control IgG derived from the same species were added to the samples and incubated overnight at 4 °C. Resuspended Protein A-Sepharose beads were then added to the samples and incubated for 3 h at 4 °C with slow rotation to precipitate the immune complexes. The supernatant was discarded, and the precipitate was retained and washed 5 times. Finally, the precipitated complexes were eluted twice with 40 µL of elution buffer, to which 10 µL of alkaline neutralization buffer and 23 µL of 5 × sample buffer were then added. The samples were boiled in water for 8 min and subsequently stored at –80 °C for analysis by Western blot.

The immunoprecipitation (IP) procedure used for the preparation of samples for Mass Spectrometry (MS) was the same as that described above. The IP samples from each group were electrophoresed to obtain gel strips, and the peptides in these strips were then enzymatically hydrolyzed. The hydrolyzed peptides were separated by column chromatography and subsequently injected into a tandem MS for primary and secondary MS analyses.

2.10 Transmission Electron Microscopy

Ventricular cardiomyocytes pretreated with high glucose were fixed with 3.0% glutaraldehyde and 1.5% paraldehyde, washed 3 times with PBS, and finally fixed with 1% osmium tetroxide for 1 h to produce osmium black. Samples were then dehydrated with ethanol and embedded in epoxy resin. A transmission electron microscope (H-7650, Tokyo, Japan) was then used to observe the number of myocardial autophagosomes and autophagolysosomes in myocardial tissue, as well as the damage to mitochondria, endoplasmic reticulum and other organelles.

2.11 Statistical Analysis

Continuous variables were presented as the mean ± SEM. The *t* test was used for comparisons between two groups. Analysis of variance (ANOVA) was used for multiple comparisons, with the Bonferroni-corrected *t* test used for post-hoc testing. Tests for significance were always two-sided, and $p < 0.05$ was considered statistically significant. Data analysis was performed using SPSS 14.0 (SPSS, Chicago, IL, USA).

3. Results

3.1 The Expression of STING and LARP7 was Increased in Myocardial Tissue from Type 1 DCM Mice, while Autophagy was Inhibited

The expression of STING and LARP7 was evaluated in myocardial cells from a mouse model of type 1 DCM, while cardiac systolic and diastolic function were evaluated by echocardiography. The systolic function index in the T1DM group was significantly lower than in the control group. High glucose levels induced LV enlargement. Meanwhile, the E/A ratio was markedly decreased in the T1DM group, indicated the mice had cardiac dias-

tolic dysfunction (Fig. 1A). In addition, the expression of STING and LARP7 in the myocardial tissue of mice from the T1DM group was significantly higher than in the control group (Fig. 1B–E). This finding was further confirmed by Western blot analysis, which revealed significant upregulation of the upstream signaling molecule cGAS and downstream effector molecule INF-β (Fig. 1H). Immunohistochemistry results showed significantly lower expression of LC3 in myocardial tissue from the T1DM group compared to the control group, indicating inhibition of autophagy (Fig. 1F). Importantly, the myocardial tissue showed myocardial fibrosis, which is a typical pathological feature of DCM (Fig. 1G). These results suggest that LARP7 and STING may play an important role in the pathogenesis of DCM.

3.2 High Glucose Induced the Expression and Activation of STING in Cardiomyocytes

Western blot analysis showed that the expression and activation levels of STING were significantly upregulated in the HG group. This effect occurred in parallel with increases in α-SMA and Cl-caspase3 (Fig. 2A). The expression of α-SMA in cardiomyocytes was further evaluated by immunofluorescence, while cardiomyocyte apoptosis was evaluated using the DNA ladder assay. The results were similar to those of Western blot analysis. Interestingly, the inhibition of STING using C-176 significantly ameliorated high glucose-induced cardiomyocyte fibrosis and apoptosis (Fig. 2B,C). In summary, high glucose caused cardiomyocyte fibrosis and apoptosis via the accumulation and activation of STING.

3.3 High Glucose Disrupted the STING-Triggered Autophagy "Negative Feedback Loop"

STING contains 7 regions (LIR1-7) that bind directly to the autophagy molecule LC3. This region induces LC3 lipidation and activates autophagy (Fig. 3A). To explore the effect of high glucose on autophagy, immunofluorescence colocalization was used to study the intracellular expression of LC3 and STING. LC3 expression and autophagy were lower in the HG group compared to the control group (Fig. 3B). COIP experiments further confirmed that high glucose reduced the binding ability of LC3 to STING (Fig. 3C). Transmission electron microscopy revealed the presence of significantly fewer autophagosomes, autophagolysosomes, and lysosomes in cardiomyocytes from the HG group compared to the control group. In addition, many of the mitochondria were swollen, damaged, and ruptured (Fig. 3D). Together, these results indicate that high glucose inhibits autophagy. This was further confirmed by Western blot analysis, which showed a significant decrease in the expression of autophagy signature proteins such as LC3II/I, Beclin-1 and P62 in NMVCMs treated with high glucose (Fig. 3E). Treatment of cardiomyocytes with the autophagy inhibitor 3-MA significantly increased the expression of STING in the cytoplasm. This was accompanied by cardiomyocyte shrinkage and poor cytoskeletal continuity. The number of apoptotic cardiomyocytes detected by the TUNEL assay was also significantly increased (Fig. 3F–I). In summary, high glucose interfered with STING degradation through the autophagy-lysosomal pathway by inhibiting the binding of STING to LC3. This resulted in accumulation of STING, leading to structural damage and increased cardiomyocyte apoptosis.

3.4 The Interaction between LARP7 and STING Aggravated Myocardial Injury

To directly explore the role of free LARP7 in DCM, the expression of LARP7 and STING were inhibited with siRNA and C-176, respectively. Western blot results showed that STING expression was significantly upregulated in the HG group. In the groups in which LARP7 or STING were inhibited, activation of the STING pathway was attenuated compared with the HG group, and cardiomyocyte apoptosis was reduced. The inhibition of LARP7 by siRNA following the inhibition of STING by C-176 had a more obvious inhibitory effect on the STING pathway (Fig. 4A). In addition, cardiomyocyte apoptosis was further reduced. These findings suggest that a regulatory mechanism between free LARP7 and STING mediates the expression and activation of STING, thereby aggravating cardiomyocyte damage.

MS analysis of three important molecules in the STING signaling pathway, cGAS-STING-TBK1, revealed a very high abundance of LARP7 in the final STING IP solution compared with the negative control (Fig. 4B). COIP experiments confirmed that both exogenously overexpressed STING and endogenous STING interacted with LARP7, and that high glucose enhanced this interaction (Fig. 4C). Next, LARP7 and STING were fluorescently labeled to visualize their intracellular localization. After high glucose treatment, a large amount of LARP7 was observed to translocate from the nucleus to the cytoplasm, where it colocalized with STING (Fig. 4D). Taken together, these results indicate that high glucose induced the intracellular translocation of LARP7, and that its interaction with STING led to accumulation in the cytoplasm where it mediated cardiomyocyte apoptosis.

3.5 LARP7 Mediates Myocardial Injury by Inhibiting the STING-Dependent Autophagy-Lysosomal Negative Feedback Loop

To further explore the mechanism by which LARP7 and STING interact to induce myocardial injury, the expression of LARP7 was first inhibited with siRNA. STING was then overexpressed via 3$\times$ Flag-STING plasmid transfection. As shown in Fig. 5A–D, inhibition of LARP7 caused the expression and activation of STING to be significantly lower than in the control and HG groups. In addition, LARP7 inhibition mitigated the activation effect caused by exogenous overexpression of STING, and alleviated apoptosis induced by the upregulation of STING. These find-

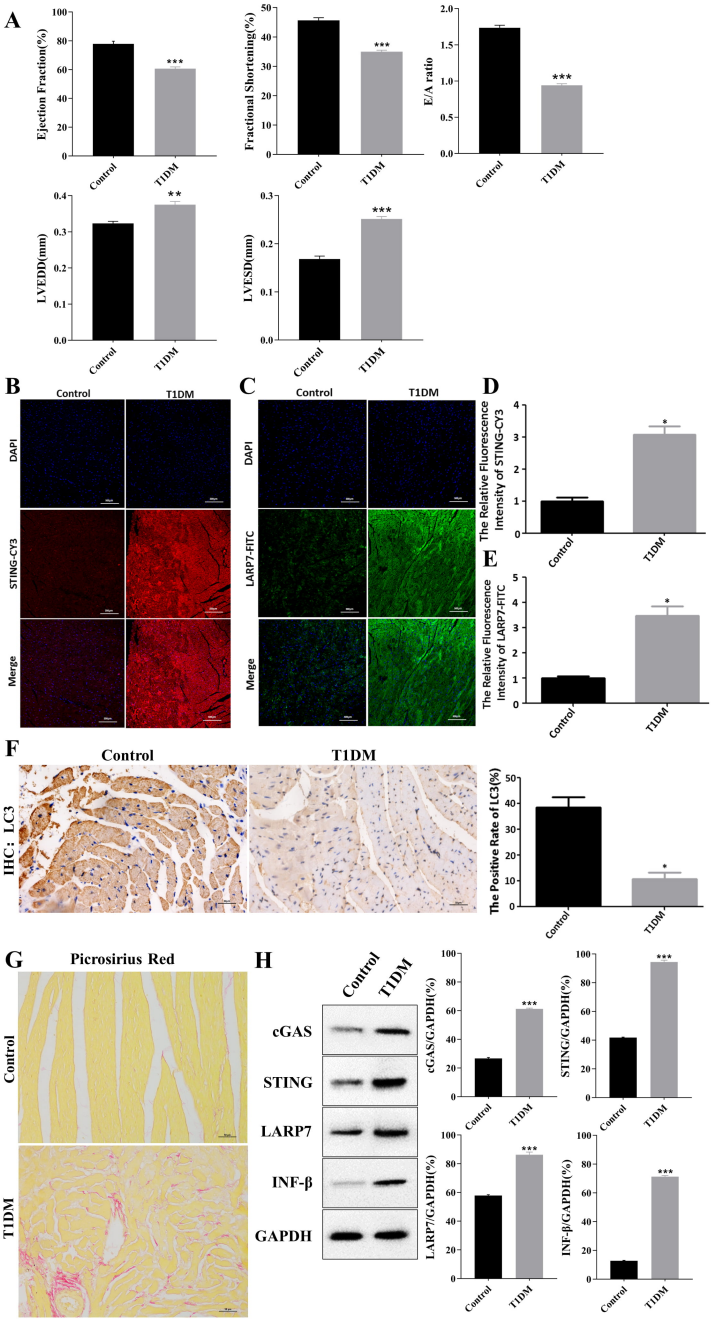

Fig. 1. Increased expression of STING and LARP7 in the myocardial tissue of mice with type 1 DCM, and inhibition of autophagy. (A) High glucose levels induced systolic and diastolic dysfunction in T1DM mice. Bar charts show decreased EF, FS, left ventricular end-diastolic internal diameter (LVEDD), left ventricular end-systolic internal diameter (LVESD) and E/A ratio after STZ injection. $^{**}p < 0.01$ and $^{***}p < 0.001$, n = 6, (mean ± SEM). (B–E) The mouse model of type 1 DCM was established by continuous intraperitoneal injection of streptozotocin (STZ). The myocardial tissue was then harvested and immunofluorescently labeled with STING-CY3 and LARP7-FITC. Differential expression of STING-CY3 and LARP7-FITC between the T1DM and control groups was then evaluated. STING-CY3 emits red fluorescence, LARP7-FITC emits green fluorescence (scale bar = 500 μm). Two-tailed Student *t* test; $^{*}p < 0.05$ *vs.* the control group, n = 3, (mean ± SEM). (F) Immunohistochemistry was used to visualize the expression of LC3 in mouse cardiomyocytes (scale bar = 50 μm). Two-tailed Student *t* test; $^{*}p < 0.05$ *vs.* the control group, n = 3, (mean ± SEM). (G) Picrosirus red staining of mouse myocardial tissue (scale bar = 50 μm). (H) Western blot results for cGAS, STING, LARP7 and INF-β in mice. Two-tailed Student *t* test; $^{***}p < 0.001$, n = 6, (mean ± SEM). STING, Stimulator of Interferon Genes; LARP7, La ribonucleoprotein domain family member 7; DCM, Diabetic Cardiomyopathy; T1DM, Type 1 Diabetes Mellitus; EF, Ejection Fraction; FS, Fractional Shortening; STING-CY3, STING-Cyanine 3; LARP7-FITC, LARP7-Fluorescein Isothiocyanate; LC3, Light Chain 3; cGAS, cyclic GMP–AMP synthase; GAPDH, Glyceraldehyde-3-phosphate dehydrogenase; E/A ratio, Early peak/Artial peak ratio.

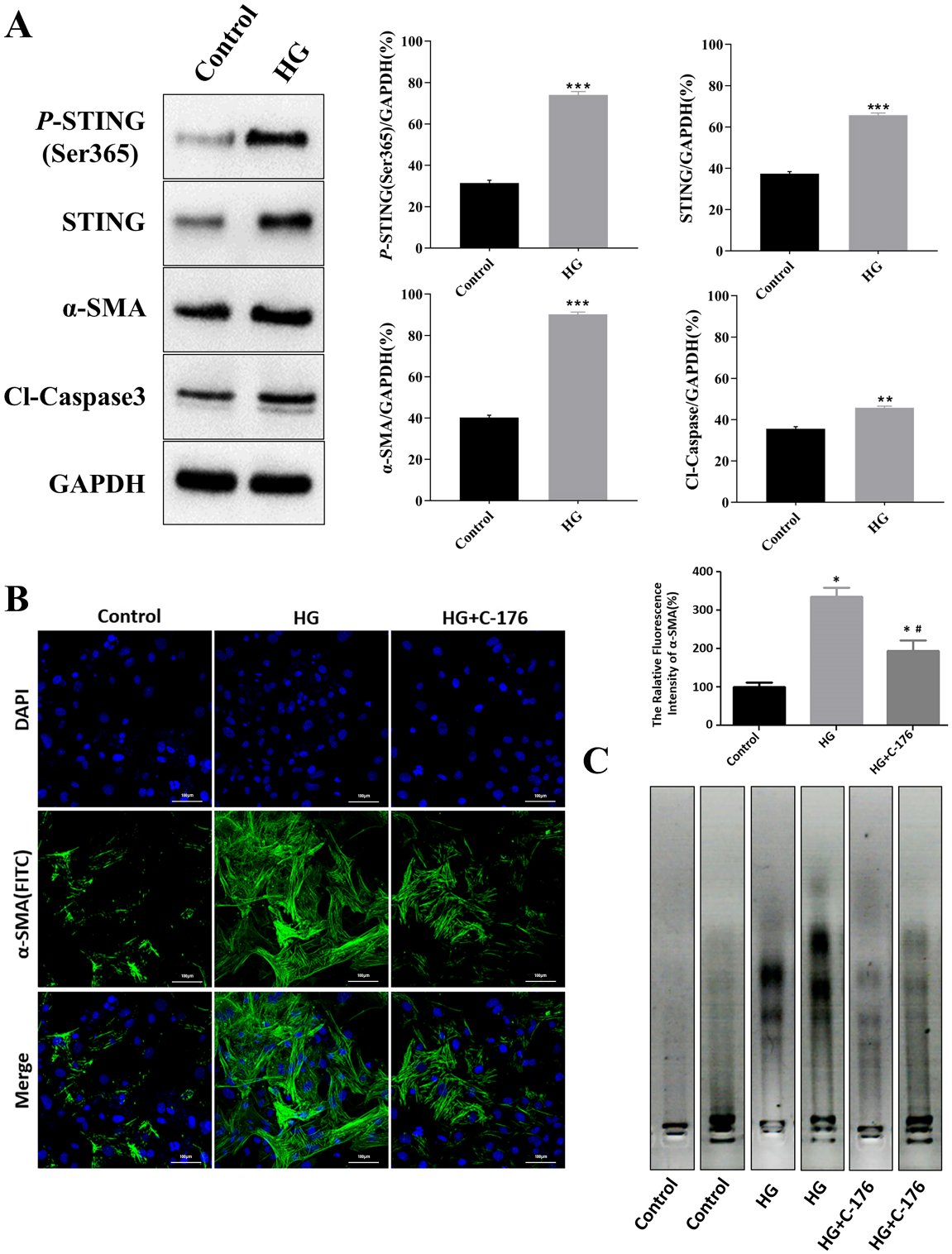

Fig. 2. High glucose enhanced the expression and activation of STING in cardiomyocytes. (A) Western blot results for STING, p-STING, α-SMA and Cl-caspase3 in NMVCMs treated with high glucose. Two-tailed Student *t* test; $^{**}p < 0.01$ and $^{***}p < 0.001$, n = 6, (mean $\pm$ SEM). (B) Immunofluorescence staining results for α-SMA in cardiomyocytes treated with high glucose and the STING inhibitor C-176 (scale bar = 100 μm). One-way ANOVA with the Bonferroni-corrected *t* test; $^{*}p < 0.05$ *vs.* control group, $^{\#}p < 0.05$ *vs.* HG group, n = 8, (mean $\pm$ SEM). (C) DNA ladder assay was used to evaluate cardiomyocyte apoptosis under different treatment conditions, which was spliced together from two repeated experiments. α-SMA, α-smooth muscle actin; HG, High Glucose; DAPI, 4′,6-diamidino-2-phenylindole.

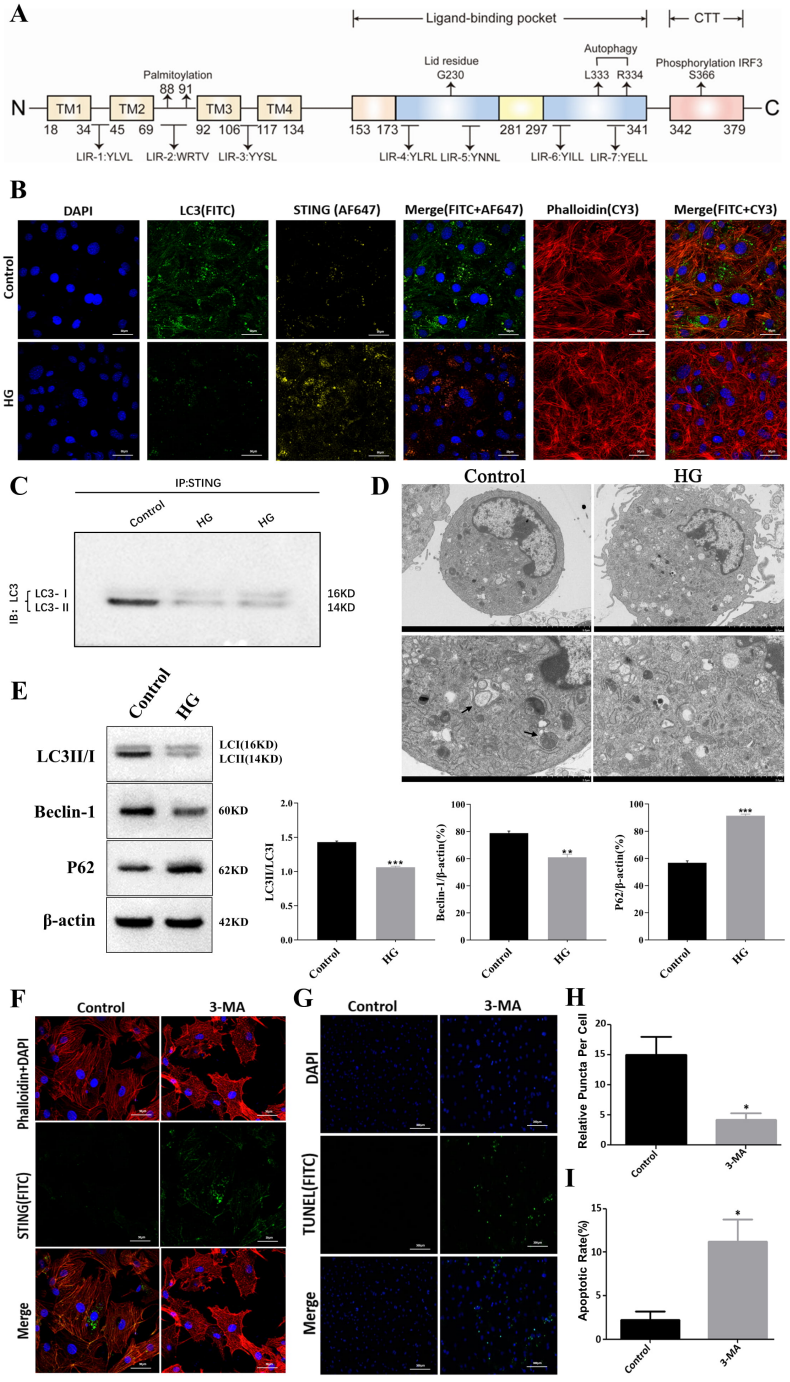

Fig. 3. High glucose levels disrupted the STING-triggered autophagy "negative feedback loop". (A) Molecular structure of STING. (B) Immunofluorescence colocalization of STING and LC3 in NMVCMs treated with high glucose: green fluorescent particles represent LC3, yellow fluorescent particles represent STING, and yellow fluorescent particles that overlap with green fluorescent particles suggest that STING directly interacts with LC3 (scale bar = 50 μm). (C) Coimmunoprecipitation (COIP) results for LC3 and STING. (D) TEM image of cardiomyocytes treated with high glucose. The black arrow represents autophagolysosomes (scale bar = 5 μm (overview); scale bar = 2 μm (inset)). (E) Western blot results for LC3II/I, Beclin-1 and P62 in NMVCMs treated with high glucose. Two-tailed Student *t* test; $^{**}p < 0.01$ and $^{***}p < 0.001$, n = 6, (mean ± SEM). (F–I) NMVCMs were pretreated with the autophagy initiation inhibitor 3-methyladenine (3-MA). The expression of STING in cardiomyocytes was then assessed by immunofluorescence, and the morphology of the cardiomyocyte cytoskeleton was assessed by phalloidin staining (scale bar = 30 μm). Two-tailed Student *t* test, $^{*}p < 0.05$ *vs.* control group, n = 8, (mean ± SEM); apoptotic cardiomyocytes were detected using the TUNEL assay (scale bar = 300 μm). Two-tailed Student *t* test, $^{*}p < 0.05$ *vs.* control group, n = 6, (mean ± SEM).

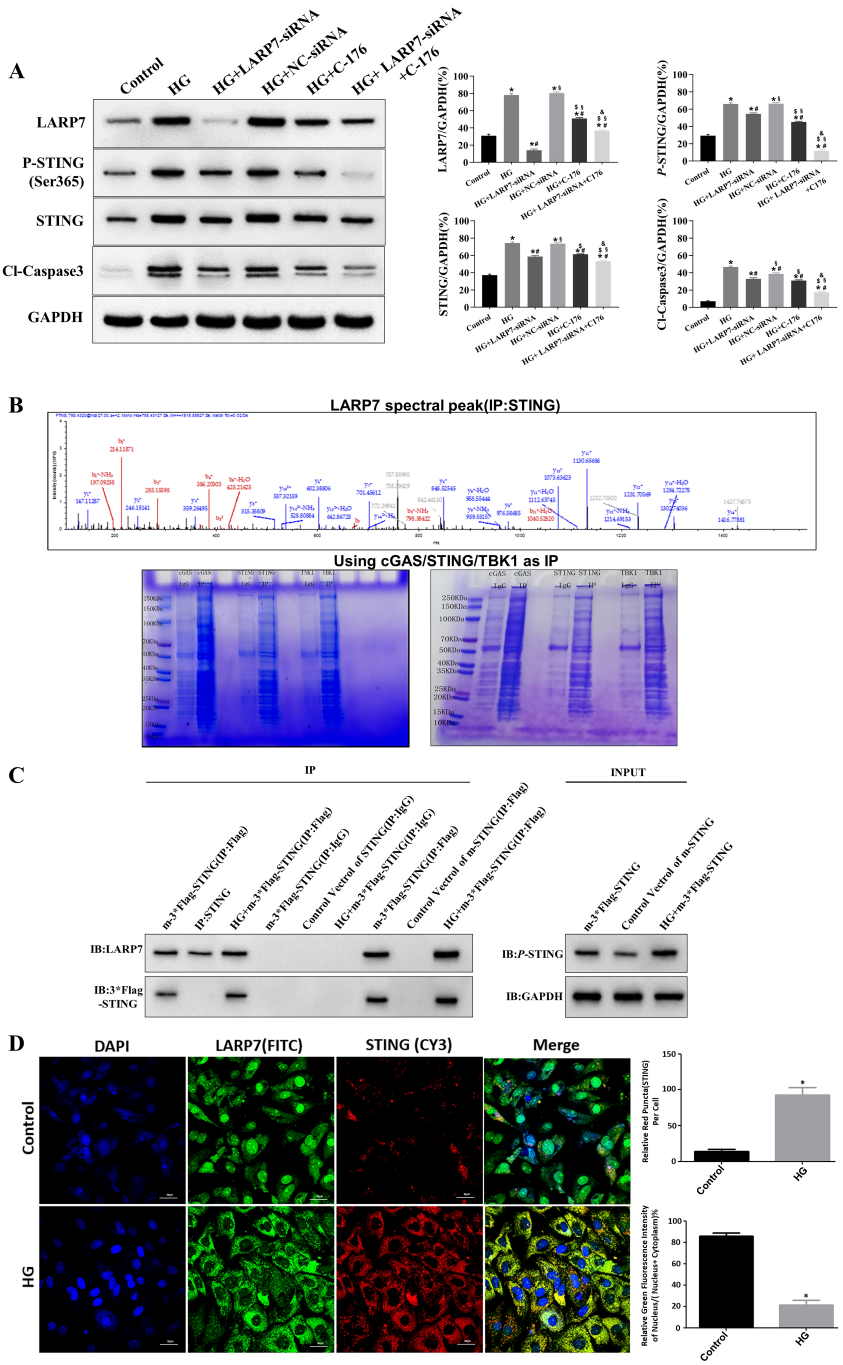

Fig. 4. LARP7 translocates from the nucleus to the cytoplasm, where its interaction with STING results in the aggravation of myocardial injury. (A) Western blot results for LARP7, STING, p-STING, and Cl-caspase3 in NMVCMs in which the expression of LARP7 and STING was inhibited by siRNA and C-176, respectively. One-way ANOVA with the Bonferroni-corrected *t* test; $^{*}p < 0.05$ *vs.* control group, $^{\#}p < 0.05$ *vs.* HG group, $^{\$}p < 0.05$ *vs.* HG+LARP7-siRNA group, $^{\$}p < 0.05$ *vs.* HG+NC-siRNA group, $^{\&}p < 0.05$ *vs.* HG+C-176 group, n = 4, (mean ± SEM). (B) Immunoprecipitation (IP) was performed for three important molecules in the STING signaling pathway: cGAS-STING-TBK1. The final solution obtained after IP was subjected to electrophoresis, and the gel strips obtained by electrophoresis were then subjected to mass spectrometry (MS). (C) COIP experiment results confirmed that both exogenously over-expressed STING (transfected with the 3×Flag-STING plasmid, IP: Flag) and endogenous STING (IP: STING) interacted with LARP7. (D) After high glucose treatment, LARP7 and STING in cardiomyocytes were labeled using an immunofluorescence double-labeling colocalization method. The green fluorescent particles represent LARP7, the red fluorescent particles represent STING, and overlapping of the two appear as yellow fluorescent particles (scale bar = 50 μm). Two-tailed Student *t* test; $^{*}p < 0.05$ *vs.* control group, n = 6, (mean ± SEM).

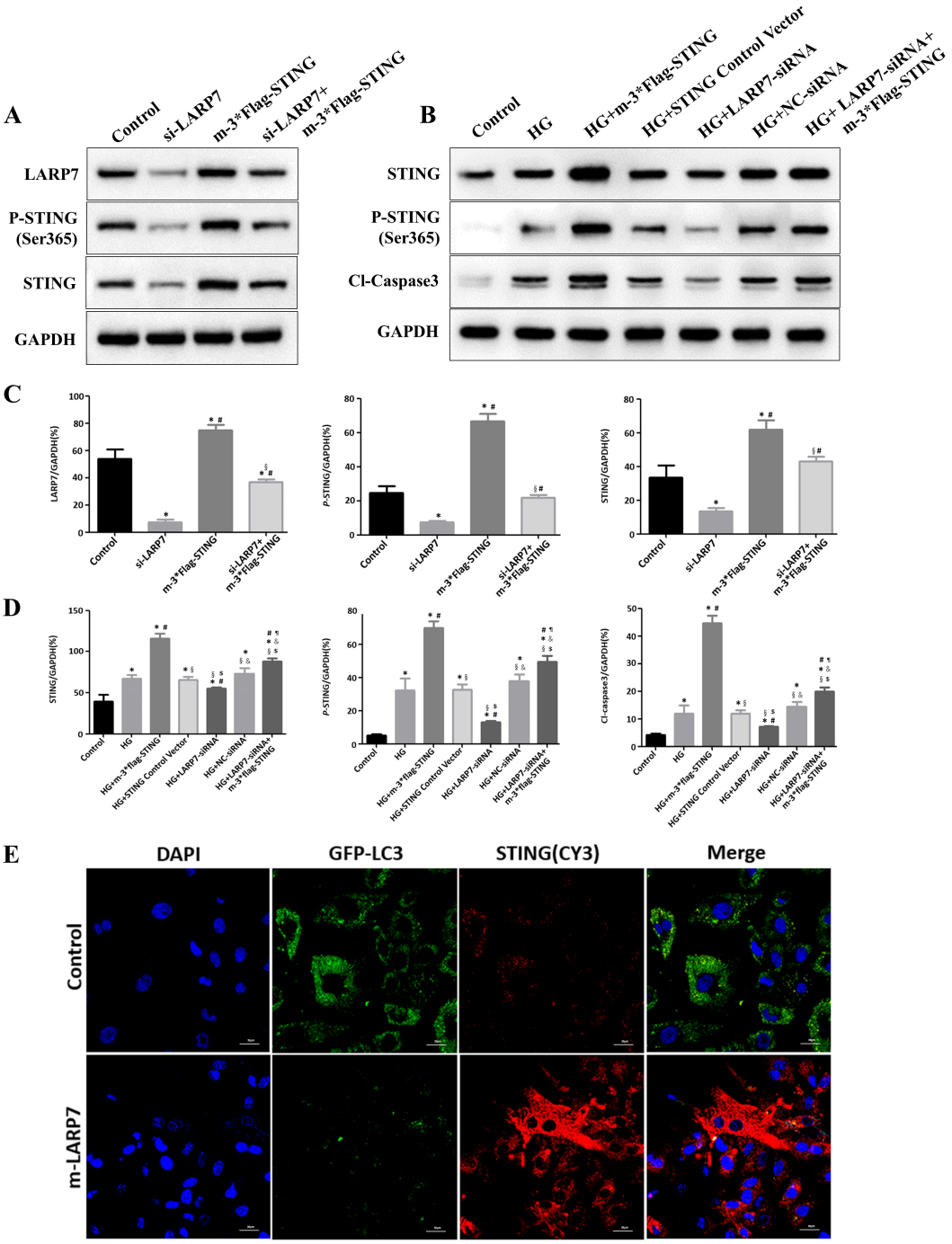

Fig. 5. LARP7 mediates myocardial injury by inhibiting the autophagy-lysosomal degradation pathway. (A,C) Mouse cardiomyocytes were treated with siLARP7, m-3*Flag-STING, or siLARP7+m-3*Flag-STING. Western blot analysis was then performed on LARP7, STING, and p-STING (Ser365). One-way ANOVA with the Bonferroni-corrected *t* test; $*p < 0.05$ *vs.* control, $^{\#}p < 0.05$ *vs.* si-LARP7, $^{\S}p < 0.05$ *vs.* m-3*Flag-STING, n = 6, (mean ± SEM). (B,D) An *in vitro* model of ventricular cardiomyocytes with type 1 diabetes mellitus was established with high glucose. The above procedures were then repeated to evaluate the expression of STING, p-STING (Ser365) and Cl-caspase3. One-way ANOVA with the Bonferroni-corrected *t* test; $*p < 0.05$ *vs.* control group, $^{\#}p < 0.05$ *vs.* HG group, $^{\S}p < 0.05$ *vs.* HG+m-3*Flag-STING group, $^{\$}p < 0.05$ *vs.* HG+STING control vector group, $^{\&}p < 0.05$ *vs.* HG+ LARP7-siRNA group, $^{\P}p < 0.05$ *vs.* HG+NC-siRNA group, n = 4, (mean ± SEM). (E) LARP7 was first upregulated and then the expression and localization of LC3 and STING in cardiomyocytes was detected using an immunofluorescence colocalization assay. Green fluorescent particles represent GFP-LC3 and GFP-LC3-labeled autophagosomes, red fluorescent particles represent STING, and yellow dots are the result of the overlapping of red dots and green dots, representing the colocalization of GFP-LC3 and STING (scale bar = 30 μm).

ings indicate that LARP7 regulates the STING pathway at an upstream location. Next, the expression and localization of LC3 and STING in cardiomyocytes were assessed following the upregulation of LARP7 expression. This revealed a significant decrease in LC3 in cardiomyocytes, accompanied by the accumulation of intracellular STING and reduced colocalization with LC3 (Fig. 5E). Together, the above results indicate that LARP7 blocks the degradation of STING by disrupting the STING-triggered autophagy-lysosomal "negative feedback loop". This results in the accumulation and overactivation of STING in cardiomyocytes, eventually causing cardiomyocyte damage.

4. Discussion

To our knowledge, this is the first study to investigate the role and mechanism of LARP7 in glucose-induced cardiac dysfunction, apoptosis and fibrosis. The main finding of this research is that high glucose induces the expression and activation of STING in ventricular myocytes, and inhibits the degradation of STING through the autophagy-lysosomal pathway. In addition, high glucose levels cause LARP7 to dissociate from the 7SK RNP complex and translocate to the cytoplasm where it interacts with STING. This inhibits the degradation of STING and causes it to accumulate and to activate downstream signaling pathways, resulting in cardiac dysfunction, fibrosis and apoptosis. Inhibition of STING or LARP7 expression significantly ameliorated high glucose-induced myocardial injury.

STING is an important signal transduction molecule and has been implicated in various diseases [25–27]. Under the action of pathogenic factors, STING becomes hyperactivated and initiates a downstream signaling cascade that induces the overexpression of IFN-I and proinflammatory cytokines [28]. STING can also trigger a fibrotic cascade, resulting in increased fibrosis in multiple tissues and organs throughout the body, including the heart [29–31]. Moreover, it can activate downstream pathways and is also associated with the induction of apoptosis [32]. The results of the present study showed that high glucose induced increased expression and activation of STING in mouse cardiomyocytes, accompanied by increased cardiomyocyte fibrosis and apoptosis. Myocardial fibrosis can impair diastolic and systolic function and eventually lead to refractory heart failure. Most cardiomyocytes are terminally differentiated cells with a limited proliferative capacity. An apoptosis rate of just 0.1% can reduce the number of cardiomyocytes by 37% within one year [33,34]. Based on this, activation of the STING pathway may cause myocardial injury in the process of DCM by mediating cardiomyocyte apoptosis and fibrosis. The reduction in myocardial fibrosis and apoptosis after treating cells with C-176 supports this inference.

Under physiological conditions, STING can be degraded through various pathways after fulfilling its signal transduction function, thereby avoiding tissue damage caused by excessive activation [35,36]. Several previous studies in diabetic mice have demonstrated the role of impaired proteasome activity in pathological cardiac remodeling. However, the aim of the current study was to further explore the pathogenic mechanism of the autophagy-lysosomal "negative feedback loop" in DCM. First, we confirmed that STING binds to LC3 in cardiomyocytes, thereby triggering the autophagy-lysosomal "negative feedback loop". However, after 3-MA was administered to inhibit autophagy, significant accumulation of STING was observed in cardiomyocytes. This was accompanied by aggravation of cardiomyocyte injury and a significant increase in the number of apoptotic cells. The above results confirm the important role of autophagy in the degradation of STING. The expression of LC3 in cardiomyocytes from the HG group was significantly lower than in cardiomyocytes from the control group. Transmission electron microscopy further confirmed that high glucose inhibited autophagy, and this was accompanied by significant cardiomyocyte damage. Collectively, these results indicate that high glucose inhibits the STING-dependent autophagy–lysosomal "negative feedback loop".

This study found a significant increase in LARP7 expression in high glucose-induced mouse ventricular myocytes. Immunofluorescence colocalization revealed that a large amount of LARP7 translocated from the nucleus to the cytoplasm and was completely colocalized with STING, thus revealing a strong interaction between LARP7 and STING. Previous studies have reported that LARP7 plays an important role in stabilizing the 7SK complex and regulating transcription elongation. In the present study, we hypothesised that LARP7 plays an important role in high glucose-induced cardiomyocyte injury once it is released into the cytoplasm. The results of MS and COIP experiments confirmed that LARP7 can indeed interact with STING, and that high glucose strengthens this interaction. Additional experiments found that inhibiting LARP7 not only decreased apoptosis induced by high glucose, but also attenuated the activation effect caused by upregulating STING. These findings indicate that LARP7 plays a key regulatory role upstream of STING. The decreased expression of LC3 molecules observed after the upregulation of LARP7 expression suggests the existence of a specific regulatory mechanism. This was supported by the results of *in vivo* animal experiments. LARP7 inhibits the STING-dependent autophagy-lysosomal "negative feedback loop", thereby causing the accumulation and overactivation of STING. This promotes cardiomyocyte apoptosis and fibrosis, which may contribute to the development of DCM.

The immunomodulatory effect of STING is currently an active area of research in the field of tumor immunotherapy, with some drugs now undergoing clinical trials. Our study also suggests that regulating the expression of LARP7 and STING may help in the treatment of DCM. However, the expression of STING was found to vary in different disease stages of DCM. In the early stage, STING expression is down-regulated due to the overactivation of au-

tophagy. In contrast, inhibition of autophagy during the middle and late stages causes STING to accumulate. These specific pathogenic characteristics may determine stage differences in treatment. For example, Irisin can alleviate cardiomyocyte apoptosis and myocardial damage by regulating STING expression [37], whereas Metrnl negatively regulates the cGAS and STING pathways and exerts an antidiabetic effect by promoting the degradation of STING after ubiquitination modification [38]. These contrasting treatment strategies suggest that tailoring the treatment to different disease stages is likely to present a major challenge. More experiments are needed to fully explore the characteristics of DCM, thereby allowing better targeted treatment.

In addition to the effects of different disease stages, it is generally accepted that the autophagic responses are distinctly different in type 1 and type 2 DM, whereas cardiac autophagic activity is enhanced in T1DM, it is suppressed in T2DM [39]. In T1DM, ATP deficiency caused by metabolic disorders or AMP accumulation activates AMPK to initiate autophagy. The main characteristic of T1DM is insulin deficiency, and insulin is known to inhibit autophagy by activating the PI3K-Akt/PKB-mTORC1 pathway [40]. T2DM hearts show the opposing conditions regarding autophagy [41,42]. High intracellular nutrient energy status lead to suppression of autophagy, which shows as the inhibition of autophagosome maturation and reduced lysosomal activity. However, diametrically opposite reports do exist. For example, decreased AMPK activity and subsequent reduction in cardiac autophagy are observed in diabetic OVE26 mice [43]. Such results are same as our study. Furthermore, Zang *et al*. [44] demonstrated that cardiac autophagic flux is intact at 3 months but is dramatically suppressed at 6 months after onset of diabetes. The results suggest that T1DM can induce glucose-dependent cardiomyocyte death by inhibiting myocardial autophagy over time. Therefore, we suggest that the different results might be related to the autophagy flux assay criteria and the different stages of mouse model construction between the studies. Further investigation is warranted regarding this issue.

Taken together, our evidence indicates that LARP7 is a key molecule in high glucose-induced cardiomyocyte injury. It exerts a pathogenic role by interfering with the STING-dependent autophagy-lysosomal "negative feedback loop". Inhibition of STING and LARP7 confers a significant cardioprotective effect, and hence the targeting of these proteins may be an effective therapeutic strategy to improve DCM.

5. Conclusions

Our study demonstrated that under high glucose conditions, LARP7 damages mouse cardiomyocytes by inhibiting STING-dependent autophagy-lysosomal degradation pathways. Targeted inhibition of LARP7 or STING expression may be a potential therapeutic strategy for DCM.

Availability of Data and Materials

Data presented in this study are contained within this article and in the **Supplementary Material**, or are available upon request to the corresponding author.

Author Contributions

JS and ZW contributed to the preliminary data analysis, interpretation, and manuscript writing. YD participated in the research design, CL and SZ provided help on the feeding of experimental animals and the construction of animal models. JD participated in the research design, provided experimental funding as well as supervision of the entire research process. All authors have participated sufficiently in the work to take public responsibility for appropriate portions of the content and agreed to be accountable for all aspects of the work in ensuring that questions related to its accuracy or integrity. All authors read and approved the final manuscript. All authors contributed to editorial changes in the manuscript.

Ethics Approval and Consent to Participate

All experiments were carried out in accordance with the Guide for the Care and Use of Laboratory Animals (Department of Health and Human Services, Publication No.[NIH] 86–23), and were approved by Animal Experimentation Committee of the Second Affiliated Hospital of Xi'an Jiaotong University (Shaanxi, approved number XJTUAE2022-374).

Acknowledgment

Not applicable.

Funding

This research received no external funding.

Conflict of Interest

The authors declare no conflict of interest.

Supplementary Material

Supplementary material associated with this article can be found, in the online version, at https://doi.org/10.31083/j.fbl2907274.

References

[1] Deng J, Wu G, Yang C, Li Y, Jing Q, Han Y. Rosuvastatin attenuates contrast-induced nephropathy through modulation of nitric oxide, inflammatory responses, oxidative stress and apoptosis in diabetic male rats. Journal of Translational Medicine. 2015; 13: 53.

[2] Cosentino F, Bhatt DL, Marx N, Verma S. The year in cardiovascular medicine 2021: diabetes and metabolic disorders. European Heart Journal. 2022; 43: 263–270.

[3] Aroda VR, Taub PR, Stanton AM. Diabetes With Cardiomyopathy: At the Juncture of Knowledge and Prevention. Journal of the American College of Cardiology. 2021; 78: 1599–1602.

[4] Schirone L, Forte M, Palmerio S, Yee D, Nocella C, Angelini F, *et al*. A Review of the Molecular Mechanisms Underlying the Development and Progression of Cardiac Remodeling. Oxidative Medicine and Cellular Longevity. 2017; 2017: 3920195.
[5] Tan Y, Zhang Z, Zheng C, Wintergerst KA, Keller BB, Cai L. Mechanisms of diabetic cardiomyopathy and potential therapeutic strategies: preclinical and clinical evidence. Nature Reviews. Cardiology. 2020; 17: 585–607.
[6] Deng J, Han Y, Sun M, Tao J, Yan C, Kang J, *et al*. Nanoporous CREG-eluting stent attenuates in-stent neointimal formation in porcine coronary arteries. PloS One. 2013; 8: e60735.
[7] Te Riet L, van Esch JHM, Roks AJM, van den Meiracker AH, Danser AHJ. Hypertension: renin-angiotensin-aldosterone system alterations. Circulation Research. 2015; 116: 960–975.
[8] Domizio JD, Gulen MF, Saidoune F, Thacker VV, Yatim A, Sharma K, *et al*. The cGAS-STING pathway drives type I IFN immunopathology in COVID-19. Nature. 2022; 603: 145–151.
[9] Hopfner KP, Hornung V. Molecular mechanisms and cellular functions of cGAS-STING signalling. Nature Reviews. Molecular Cell Biology. 2020; 21: 501–521.
[10] Hu H, Zhao R, He Q, Cui C, Song J, Guo X, *et al*. cGAS-STING mediates cytoplasmic mitochondrial-DNA-induced inflammatory signal transduction during accelerated senescence of pancreatic β-cells induced by metabolic stress. FASEB Journal: Official Publication of the Federation of American Societies for Experimental Biology. 2022; 36: e22266.
[11] Yan M, Li Y, Luo Q, Zeng W, Shao X, Li L, *et al*. Mitochondrial damage and activation of the cytosolic DNA sensor cGAS-STING pathway lead to cardiac pyroptosis and hypertrophy in diabetic cardiomyopathy mice. Cell Death Discovery. 2022; 8: 258.
[12] Zhong B, Zhang L, Lei C, Li Y, Mao AP, Yang Y, *et al*. The ubiquitin ligase RNF5 regulates antiviral responses by mediating degradation of the adaptor protein MITA. Immunity. 2009; 30: 397–407.
[13] Li N, Zhou H, Wu H, Wu Q, Duan M, Deng W, *et al*. STING-IRF3 contributes to lipopolysaccharide-induced cardiac dysfunction, inflammation, apoptosis and pyroptosis by activating NLRP3. Redox Biology. 2019; 24: 101215.
[14] Gui X, Yang H, Li T, Tan X, Shi P, Li M, *et al*. Autophagy induction via STING trafficking is a primordial function of the cGAS pathway. Nature. 2019; 567: 262–266.
[15] King KR, Aguirre AD, Ye YX, Sun Y, Roh JD, Ng RP, Jr, *et al*. IRF3 and type I interferons fuel a fatal response to myocardial infarction. Nature Medicine. 2017; 23: 1481–1487.
[16] Reis MB, Rodrigues FL, Lautherbach N, Kanashiro A, Sorgi CA, Meirelles AFG, *et al*. Interleukin-1 receptor-induced PGE_2 production controls acetylcholine-mediated cardiac dysfunction and mortality during scorpion envenomation. Nature Communications. 2020; 11: 5433.
[17] Hu D, Cui YX, Wu MY, Li L, Su LN, Lian Z, *et al*. Cytosolic DNA sensor cGAS plays an essential pathogenetic role in pressure overload-induced heart failure. American Journal of Physiology. Heart and Circulatory Physiology. 2020; 318: H1525–H1537.
[18] Frilander MJ, Barborič M. The Interlocking Lives of LARP7: Fine-Tuning Transcription, RNA Modification, and Splicing through Multiple Non-coding RNAs. Molecular Cell. 2020; 78: 5–8.
[19] Ji C, Bader J, Ramanathan P, Hennlein L, Meissner F, Jablonka S, *et al*. Interaction of 7SK with the Smn complex modulates snRNP production. Nature Communications. 2021; 12: 1278.
[20] Liang X, Wu S, Geng Z, Liu L, Zhang S, Wang S, *et al*. LARP7 Suppresses Endothelial-to-Mesenchymal Transition by Coupling With TRIM28. Circulation Research. 2021; 129: 843–856.
[21] Sano M, Abdellatif M, Oh H, Xie M, Bagella L, Giordano A, *et al*. Activation and function of cyclin T-Cdk9 (positive transcription elongation factor-b) in cardiac muscle-cell hypertrophy. Nature Medicine. 2002; 8: 1310–1317.
[22] Martin RD, Sun Y, MacKinnon S, Cuccia L, Pagé V, Hébert TE, *et al*. Differential Activation of P-TEFb Complexes in the Development of Cardiomyocyte Hypertrophy following Activation of Distinct G Protein-Coupled Receptors. Molecular and Cellular Biology. 2020; 40: e00048-20.
[23] Zhang M, Zhang L, Hu J, Lin J, Wang T, Duan Y, *et al*. MST1 coordinately regulates autophagy and apoptosis in diabetic cardiomyopathy in mice. Diabetologia. 2016; 59: 2435–2447.
[24] Saraste A, Pulkki K. Morphologic and biochemical hallmarks of apoptosis. Cardiovascular Research. 2000; 45: 528–537.
[25] Wassermann R, Gulen MF, Sala C, Perin SG, Lou Y, Rybniker J, *et al*. Mycobacterium tuberculosis Differentially Activates cGAS- and Inflammasome-Dependent Intracellular Immune Responses through ESX-1. Cell Host & Microbe. 2015; 17: 799–810.
[26] Gao D, Li T, Li XD, Chen X, Li QZ, Wight-Carter M, *et al*. Activation of cyclic GMP-AMP synthase by self-DNA causes autoimmune diseases. Proceedings of the National Academy of Sciences of the United States of America. 2015; 112: E5699–E5705.
[27] Zhang Y, Chen W, Wang Y. STING is an essential regulator of heart inflammation and fibrosis in mice with pathological cardiac hypertrophy via endoplasmic reticulum (ER) stress. Biomedicine & Pharmacotherapy. 2020; 125: 110022.
[28] Chen Q, Sun L, Chen ZJ. Regulation and function of the cGAS-STING pathway of cytosolic DNA sensing. Nature Immunology. 2016; 17: 1142–1149.
[29] Fang L, Ellims AH, Beale AL, Taylor AJ, Murphy A, Dart AM. Systemic inflammation is associated with myocardial fibrosis, diastolic dysfunction, and cardiac hypertrophy in patients with hypertrophic cardiomyopathy. American Journal of Translational Research. 2017; 9: 5063–5073.
[30] Luo X, Li H, Ma L, Zhou J, Guo X, Woo SL, *et al*. Expression of STING Is Increased in Liver Tissues From Patients With NAFLD and Promotes Macrophage-Mediated Hepatic Inflammation and Fibrosis in Mice. Gastroenterology. 2018; 155: 1971–1984.e4.
[31] Bai J, Cervantes C, Liu J, He S, Zhou H, Zhang B, *et al*. DsbA-L prevents obesity-induced inflammation and insulin resistance by suppressing the mtDNA release-activated cGAS-cGAMP-STING pathway. Proceedings of the National Academy of Sciences of the United States of America. 2017; 114: 12196–12201.
[32] Diner BA, Lum KK, Toettcher JE, Cristea IM. Viral DNA Sensors IFI16 and Cyclic GMP-AMP Synthase Possess Distinct Functions in Regulating Viral Gene Expression, Immune Defenses, and Apoptotic Responses during Herpesvirus Infection. mBio. 2016; 7: e01553-16.
[33] Mani K. Programmed cell death in cardiac myocytes: strategies to maximize post-ischemic salvage. Heart Failure Reviews. 2008; 13: 193–209.
[34] Wencker D, Chandra M, Nguyen K, Miao W, Garantziotis S, Factor SM, *et al*. A mechanistic role for cardiac myocyte apoptosis in heart failure. The Journal of Clinical Investigation. 2003; 111: 1497–1504.
[35] Wang Y, Lian Q, Yang B, Yan S, Zhou H, He L, *et al*. TRIM30α Is a Negative-Feedback Regulator of the Intracellular DNA and DNA Virus-Triggered Response by Targeting STING. PLoS Pathogens. 2015; 11: e1005012.
[36] Konno H, Konno K, Barber GN. Cyclic dinucleotides trigger ULK1 (ATG1) phosphorylation of STING to prevent sustained innate immune signaling. Cell. 2013; 155: 688–698.
[37] Lu L, Shao Y, Xiong X, Ma J, Zhai M, Lu G, *et al*. Irisin improves diabetic cardiomyopathy-induced cardiac remodeling by regulating GSDMD-mediated pyroptosis through MI-

TOL/STING signaling. Biomedicine & Pharmacotherapy. 2024; 171: 116007.

[38] Lu QB, Ding Y, Liu Y, Wang ZC, Wu YJ, Niu KM, *et al*. Metrnl ameliorates diabetic cardiomyopathy via inactivation of cGAS/STING signaling dependent on LKB1/AMPK/ULK1-mediated autophagy. Journal of Advanced Research. 2023; 51: 161–179.

[39] Kanamori H, Takemura G, Goto K, Tsujimoto A, Mikami A, Ogino A, *et al*. Autophagic adaptations in diabetic cardiomyopathy differ between type 1 and type 2 diabetes. Autophagy. 2015; 11: 1146–1160.

[40] Riehle C, Wende AR, Sena S, Pires KM, Pereira RO, Zhu Y, *et al*. Insulin receptor substrate signaling suppresses neonatal autophagy in the heart. The Journal of Clinical Investigation. 2013; 123: 5319–5333.

[41] Sciarretta S, Zhai P, Shao D, Maejima Y, Robbins J, Volpe M, *et al*. Rheb is a critical regulator of autophagy during myocardial ischemia: pathophysiological implications in obesity and metabolic syndrome. Circulation. 2012; 125: 1134–1146.

[42] Zhang L, Ding WY, Wang ZH, Tang MX, Wang F, Li Y, *et al*. Early administration of trimetazidine attenuates diabetic cardiomyopathy in rats by alleviating fibrosis, reducing apoptosis and enhancing autophagy. Journal of Translational Medicine. 2016; 14: 109.

[43] Xie Z, Lau K, Eby B, Lozano P, He C, Pennington B, *et al*. Improvement of cardiac functions by chronic metformin treatment is associated with enhanced cardiac autophagy in diabetic OVE26 mice. Diabetes. 2011; 60: 1770–1778.

[44] Zang H, Wu W, Qi L, Tan W, Nagarkatti P, Nagarkatti M, *et al*. Autophagy Inhibition Enables Nrf2 to Exaggerate the Progression of Diabetic Cardiomyopathy in Mice. Diabetes. 2020; 69: 2720–2734.